AIAA 80-1788R

Reliability and Accuracy Prediction for a Redundant Strapdown Navigator

J.V. Harrison,* K.C. Daly,† and E. Gai‡
The Charles Stark Draper Laboratory, Inc., Cambridge, Mass.

A comprehensive approach to the evaluation of the accuracy and reliability of a redundant navigation system is described. A Markov model of the redundant system is used to determine the probabilities of particular operational state time histories. Navigation system accuracies are associated with these state time histories through the use of a modified covariance analysis of the system's navigation errors. Suitable scalar figures of merit are used to assess the impact on performance of significant system parameters. The analysis is applied to a redundant navigator which is used to transfer a payload from launch to geosynchronous orbit.

I. Introduction

THE accuracy of navigation systems has traditionally been evaluated by means of conventional covariance analysis techniques,[1] sensitivity analyses,[2] or Monte Carlo simulations.[3] These approaches are not well suited, however, to the evaluation of the accuracy of a redundant system. This is primarily due to the fact that the operational state of a redundant system changes at random points in time, resulting in a very large ensemble of operational state time histories which must be considered. An analysis approach which accounts for the effects of the random occurrence of component failures and reconfigurations of the redundant system elements is required.

The operational state of a redundant system changes as system components fail and as failure detection and identification (FDI) decisions are made. A Markov model of the redundant system and its associated FDI algorithms can be used to determine the probabilities of particular operational state time histories. These probabilities can be used to identify the members of the ensemble of operational state time histories which most strongly influence system performance. A linearized stochastic sensitivity analysis[4] can then be used to determine the statistics of the navigation system errors for each of the operational state time histories of interest.

The many factors which influence the accuracy of a redundant navigation system also influence the system's reliability. Conventional reliability prediction methods[5] must be augmented, therefore, in order to include these effects. A Markov model is well suited to this purpose. System reliability can be predicted by summing the probabilities of all operational state time histories which end in severely degraded performance.

The use of Markov modeling techniques to predict system performance also provides insight into the sensitivity of this performance to significant features of the system design. These techniques thus provide a systematic method of evaluating design tradeoffs and for choosing parameters such as FDI thresholds by examining the effects of these tradeoffs and choices on system accuracy and reliability.

The redundant inertial measurement unit (RIMU)[6] considered in this paper consists of five gyros and five accelerometers in a conical configuration. Three power supplies are associated with the sensors. Two of these power supplies service nonadjacent pairs of gyros and accelerometers. The third power supply services the remaining gyro and accelerometer.

The redundancy management structure consists of algorithmic FDI based on the Generalized Likelihood Test (GLT) decision functions.[7] This algorithmic FDI is supplemented by built-in tests (BITE). The GLT decision functions utilize parity vector residuals which are obtained at 100 Hz by forming linear combinations of the redundant measurements of incremental angle and velocity.

In order to reliably detect and identify sensor failures which are manifest as bias shifts in the sensor outputs, three algorithmic FDI tests are performed on the parity vector residuals. The hard FDI test is performed at 50 Hz on the average of two parity vector residuals. This test provides immediate protection from large failure magnitudes which must be screened out prior to data usage. Detected failures are immediately isolated to a pair of adjacent sensors by the hard FDI test. Thus only one detection threshold is required. The mid-FDI test is performed at 25 Hz on averaged parity vector data which have been passed through a first-order filter with a 1-s time constant. This test provides protection from moderate-sized failures. Like the hard FDI test, a single threshold is used to detect and immediately isolate these failures to an adjacent pair of sensors. A soft FDI test is performed at 2 Hz on averaged parity vector data which have been passed through a second-order filter with a 15-s time constant. Two detection thresholds are used. The smaller of these is used to detect and isolate low-level failures to a pair of adjacent sensors. The larger threshold is used to initiate isolation to a single sensor. This occurs when an isolation criterion which depends on an isolation threshold is met.

BITE consists of a number of independent tests of system-status indicators which are indicative of the health of particular system components. All BITE tests are performed at 50 Hz. A distinction is made between sensor BITE tests (e.g., loop-closure test, gyro spin motor run detection and data parity checks) and power supply BITE tests (e.g., voltage level tests). BITE coverage of power supply failures is particularly important in this system since the failure of a power supply which services a pair of sensors represents a failure mode which the algorithmic FDI tests are incapable of correctly isolating.

In the redundancy management structure, BITE tests take precedence over algorithmic FDI tests. These tests establish the validity of the sensor measurement data for subsequent algorithmic FDI tests. The hard and mid FDI tests are performed only when there are five valid sensor measurements. In addition to being performed when there are five valid measurements, the soft FDI tests continue to be performed

Presented as Paper 80-1788 at the AIAA Guidance and Control Conference, Danvers, Mass., Aug. 11-13, 1980; submitted Sept. 15, 1980: revision received Feb. 3, 1981.

*Technical Staff Member.
†Technical Staff Member. Member AIAA.
‡Technical Staff Member. Member AIAA.

Table 1 Mission phases

Phase	Description	Duration, s
1	Boost	496.5
2	Low-Earth orbit	3510
3	1st attitude maneuver and burn	249
4	Transfer orbit	16,648
5	2nd attitude maneuver and burn	385.5

Table 2 Markov model states

Model state	Operational state of system
0	Pentad, no sensor failures
1	Pentad, missed failure
2	Adjacent triad, false alarm
3	Adjacent triad, failure correctly isolated to pair of sensors
4	Adjacent triad, failure incorrectly isolated to pair of sensors
5	Quartet, failure correctly isolated to a sensor
6	Adjacent triad, FDI terminated
7	Nonadjacent triad, power supply failure covered by BITE
8	Quartet or nonadjacent triad, one failed sensor in use
9	Loss of function

Table 3 Event description

Event	Description
1	Occurrence of a sensor or power supply failure
2	Outcome of BITE test
3	Detection outcome of fast FDI test
4	Isolation outcome of fast FDI test
5	Detection outcome of soft FDI test
6	Isolation outcome of soft FDI test

after a failure has been isolated to a pair by any of the algorithmic FDI tests. This permits subsequent isolation of these failures to a single sensor.

The mission for which accuracy and reliability predictions are desired is assumed to be the launch and subsequent insertion of a satellite into geosynchronous orbit. The mission is divided into the five phases indicated in Table 1.

II. Markov Model

The Markov model of the system under consideration has ten states (see Table 2). With the exception of the zero state, each of these states represents an aggregation of more than one of the system's possible operational states. The differences between aggregated states is small, however, compared to the differences between aggregations.

The states of the Markov model are ordered in such a way that downward transitions (i.e., transitions from higher to lower numbered states) are not possible. As a result, the single-step state transition matrix P_s of the Markov model is lower triangular. Thus,

$$P_s = [p_{ij}] \qquad p_{ij} = 0 \quad \text{for} \quad i < j \tag{1}$$

The value inserted in P_s for each element p_{ij} represents the probability of a transition from state j to state i in a single time step Δt.

A time step of 0.5 s is assumed. This corresponds to a single decision interval for the 2-Hz soft FDI test. Since BITE, hard and mid-FDI tests are made more frequently, their effect over a 0.5-s interval must be approximated. The hard and mid-FDI tests are modeled as an equivalent 2-Hz fast FDI test with performance probabilities given by

$$p_{*,\text{fast}} = 1 - (1 - p_{*,\text{hard}})^{25}(1 - p_{*,\text{mid}})^{12.5} \tag{2}$$

where "*" designates detection, false alarm, or correct isolation. In these expressions, the exponents represent the

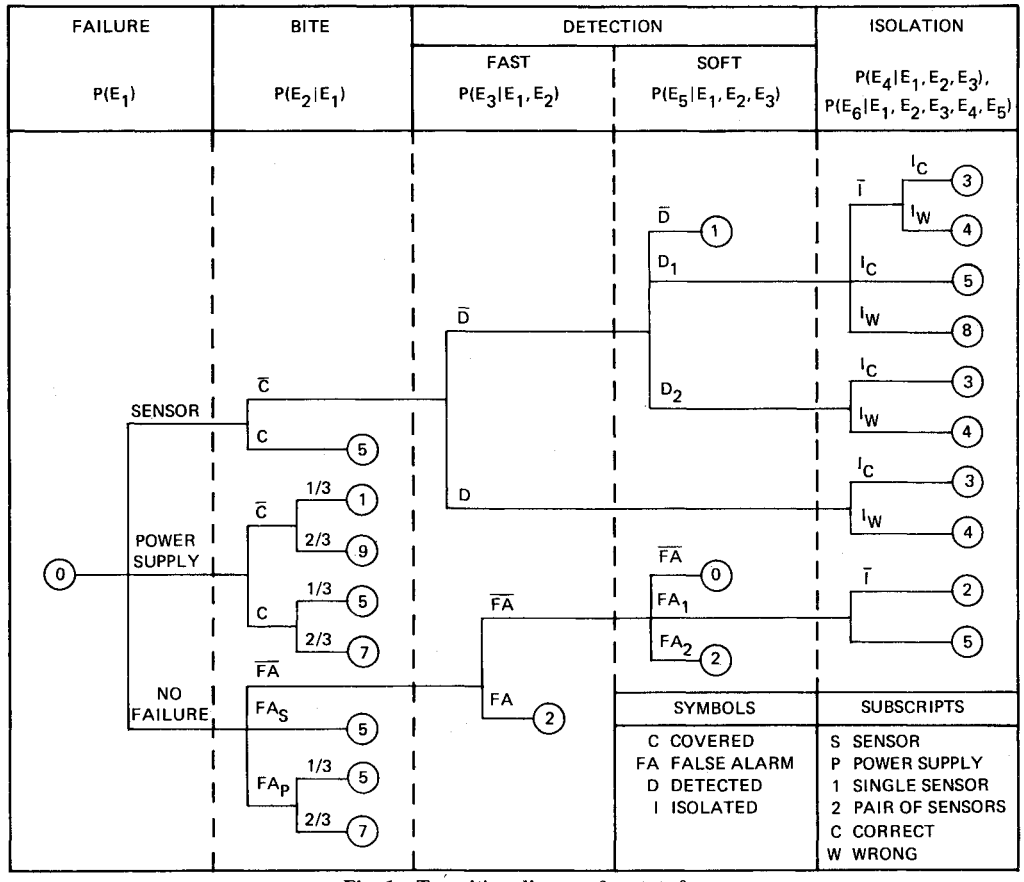

Fig. 1 Transition diagram for state 0.

average number of hard or mid-FDI tests in an 0.5-s interval. The probabilities on the right-hand side can be computed analytically by the methods of Ref. 8. The 50-Hz BITE tests are modeled as an equivalent 2-Hz BITE test with specified coverage $p_{\mathrm{COV,BITE}}$ and with a probability of false alarm $p_{\mathrm{FA,BITE}}$ given by

$$p_{\mathrm{FA,BITE}} = 1 - (1 - p'_{\mathrm{FA,BITE}})^{25} \tag{3}$$

where $p'_{\mathrm{FA,BITE}}$ is determined by analyzing the failure rates of the BITE circuitry.

The single-step state transition probabilities p_{ij} for the Markov model can be expressed in terms of the probabilities of six successive events (see Table 3). The first of these is associated with a system failure, whereas the others depend on the results of the BITE and FDI tests. The conditioning of these events is indicated in the following expression

$$p_{ij} = p(E_1)p(E_2 \mid E_1)p(E_3 \mid E_1,E_2)p(E_4 \mid E_1,E_2,E_3) \times p(E_5 \mid E_1,E_2,E_3)p(E_6 \mid E_1,E_2,E_3,E_4,E_5) \tag{4}$$

where $p(E_1)$ is determined from the failure rates of the sensors and power supplies; $p(E_2 \mid E_1)$ depends on the assumed BITE coverage and the BITE false alarm probability computed in Eq. (3); and $p(E_3 \mid E_1,E_2)$ and $p(E_4 \mid E_1,E_2,E_3)$ follow from Eq. (2) after p_D, p_{FA}, and p_{CI} are determined using the methods of Ref. 8. The remainder of the probabilites in Eq. (4) are directly computed using the methods of Ref. 8.

Equation (4) can be evaluated systematically by creating a state transition diagram for each state of the Markov model. As an example, the transition diagram for the zero state is presented in Fig. 1. The elements of P_s depend on the time step which is used, the various rates at which BITE tests and FDI tests are performed, the BITE coverage which is assumed, the failure rates assumed for system components and BITE circuitry, the sensor measurement noise which characterizes unfailed sensors, the particular detection and isolation thresholds which are specified for the algorithmic FDI, and the magnitude of the failure, if any, which is present in the system.

Once the elements of the single-step state transition matrix P_s have been determined, the multistep state transition matrix P_{ms} can be determined from

$$P_{ms} = P_s^n \tag{5}$$

where n indicates the number of decision intervals over which the elements of P_s remain time-invariant. As the dynamic environment changes during the mission, the elements of P_s change. This is due to the effect which the dynamic environment has on component failure rates and on the measurement noise which characterizes the unfailed sensors. For this reason, the mission under consideration in this paper has been divided into the five phases indicated in Table 1. During each of these phases the elements of P_s are assumed to be time-invariant. The state transition matrix P_m for the entire mission is then given by

$$P_m = \prod_{i=1}^{5} (P_{s_i})^{n_i} \tag{6}$$

where P_{s_i} is the single-step state transition matrix and n_i is the number of decision intervals in the ith phase of the mission.

III. Performance Prediction

The performance of a redundant system depends on the time history of the operational state of the system during the whole mission. The operational state may change whenever a system component fails or a false alarm occurs. These events occur at random times, and the particular state transition which occurs depends on the results of the FDI tests. In order to predict system performance, therefore, it is necessary to consider the ensemble of all possible operational state time histories. This ensemble can be reduced to a manageable size by assuming that state changes occur only at the beginning of mission phases. Each member of this reduced ensemble is called a path. These paths can be identified as

$$k:\{\alpha_1,\alpha_2,\alpha_3,\alpha_4,\alpha_5\} \tag{7}$$

where k is a uniquely assigned path number and α_i designates the state of the system at the end of phase i. Since there are ten states in the Markov model, α_i can refer to any of the 0 through 9 states.

Because not all state transitions are possible, however, the number of paths in the ensemble under consideration is limited to 847. These paths cover the spectrum from path 1:{0,0,0,0,0}, which represents the case in which neither a failure nor a false alarm occurs throughout the mission to path 847:{9,9,9,9,9}, which represents the case in which loss of function occurs in the boost phase of the mission.

The Markov model is used to determine the probability of each of the 847 paths in the ensemble. The probability associated with the path $k:\{\alpha_1,\alpha_2,\alpha_3,\alpha_4,\alpha_5\}$ is given by

$$p(k) = \prod_{j=0}^{4} p_{\alpha_{j+1},\alpha_j} \tag{8}$$

where $p_{\alpha_{j+1},\alpha_j}$ designates the probability of making a transition from state α_j to state α_{j+1} in phase $j+1$ of the mission. Thus, $p_{\alpha_{j+1},\alpha_j}$ is the (α_{j+1},α_j) element of $[P_{sj+1}]^{n_{j+1}}$. α_0 designates the initial state; in this case, zero.

The tasks of exhaustively enumerating the 847 paths in the ensemble, computing their individual probabilities using the Markov model, and ordering the members of this ensemble according to the decreasing probability of their occurrence are easily automated. This establishes a list of clearly defined operational state time histories, which is prioritized in terms of probability of occurrence.

The next step in the analysis is to obtain performance predictions. A linearized stochastic sensitivity analysis[4] can be used to determine the statistics of the redundant navigation system position and velocity errors as a function of time for each operational state time history. In addition to accounting for the effects of navigation system error sources such as initial alignment errors and the inertial sensors' static and dynamic errors, the linearized analysis also accounts for those effects that are uniquely associated with redundant systems. The effects of undetected and incorrectly isolated failures on the mean of the navigation errors, as well as the effects of reconfiguration of the redundant sensors on the propagation of both the mean and covariance of the navigation errors, are included. In evaluating the navigation error statistics for a particular path k [see Eq. (7)], transitions to the state α_i, which defines the state of the system at the end of phase i, are assumed to occur at the beginning of that phase. The effect of this assumption on the numerical results which are thus obtained is conservative.

In order to be useful for making design tradeoffs and selecting FDI thresholds, it is desirable to reduce performance predictions to a single scalar figure of merit. In the case of accuracy predictions, this can be done by interpreting the statistics of the navigation system's position and velocity errors in terms of the probability of exceeding a performance specification imposed on these errors. For the mission under consideration, a performance specification which bounds the position and velocity errors at insertion into geosynchronous orbit is assumed (see Table 4).

Given the means and covariance of the six position and velocity errors for each operational state time history, it is possible (at least conceptually) to compute the probability of exceeding the navigation system accuracy requirement

specified in Table 4. In practice, one or two of the errors dominate. By identifying the two errors for each path which, given their mean and covariance, have the highest probability of exceeding their bounds, the probability of exceeding the system accuracy requirement is easily approximated analytically.[4] This probability is designated $c(k,b)$, where the notation indicates that the probability of exceeding the accuracy requirement is interpreted as a cost which is uniquely associated with path k. The explicit dependence of $c(k,b)$ on the failure magnitude b (if any) is indicated. The expected value of $c(k,b)$ over the ensemble of paths k and failure magnitudes b is taken as the scalar figure of merit (AFOM) for accuracy.

$$\text{AFOM} = \int_B \sum_k c(k,b)p(k\,|b)p(b)\,db \tag{9}$$

In this expression, $p(k\,|b)$ designates the probability of path k obtained from the Markov model. This probability is conditioned on the failure magnitude b. In most practical cases, the density function $p(b)$ for the failure magnitude b is unknown. For a well-designed FDI system, however, the inner sum in Eq. (9) is insensitive to the assumed failure magnitude. In such cases the accuracy figure of merit reduces to

$$\text{AFOM} = \sum_k c(k)p(k) \tag{10}$$

Table 4 Navigation system accuracy requirements (3σ)

Component	Position, n.mi.	Velocity, ft/s
Tangential	55	10
Normal	35	10
Radial	44	50

Because $c(k)$ in Eq. (10) is bounded; i.e.,

$$c(k) \leq 1 \quad \text{for all } k$$

it is unnecessary to compute $c(k)$ for paths with probability $p(k)$ less than a suitably chosen lower bound. By ordering the 847 members of the ensemble of operational state time histories in terms of the decreasing probability of their occurrence, therefore, it is possible to truncate the sum indicated in Eq. (10) when $p(k)$ reaches this bound. This is advantageous, since the determination of $c(k)$ is the only task in the analysis which incurs significant computational costs.

A scalar figure of merit (RFOM) for predicting system reliability can be defined analogously to Eq. (9).

$$\text{RFOM} = \int_B \sum_{k\epsilon K} c(k,b)p(k\,|b)p(b)\,db \tag{11}$$

where K represents that subset of the 847 paths for which

$$c(k,b) = 1 \tag{12}$$

For those cases in which the inner sum of Eq. (11) is insensitive to failure magnitude, the reliability figure of merit reduces to

$$\text{RFOM} = \sum_{k\epsilon K} p(k) \tag{13}$$

IV. Numerical Results

Numerical results are presented in this section for the redundant strapdown navigation system and the geosynchronous orbit insertion mission which were described in Sec. I. The inputs to the analysis, the computational flow, and the most significant results are indicated in Fig. 2.

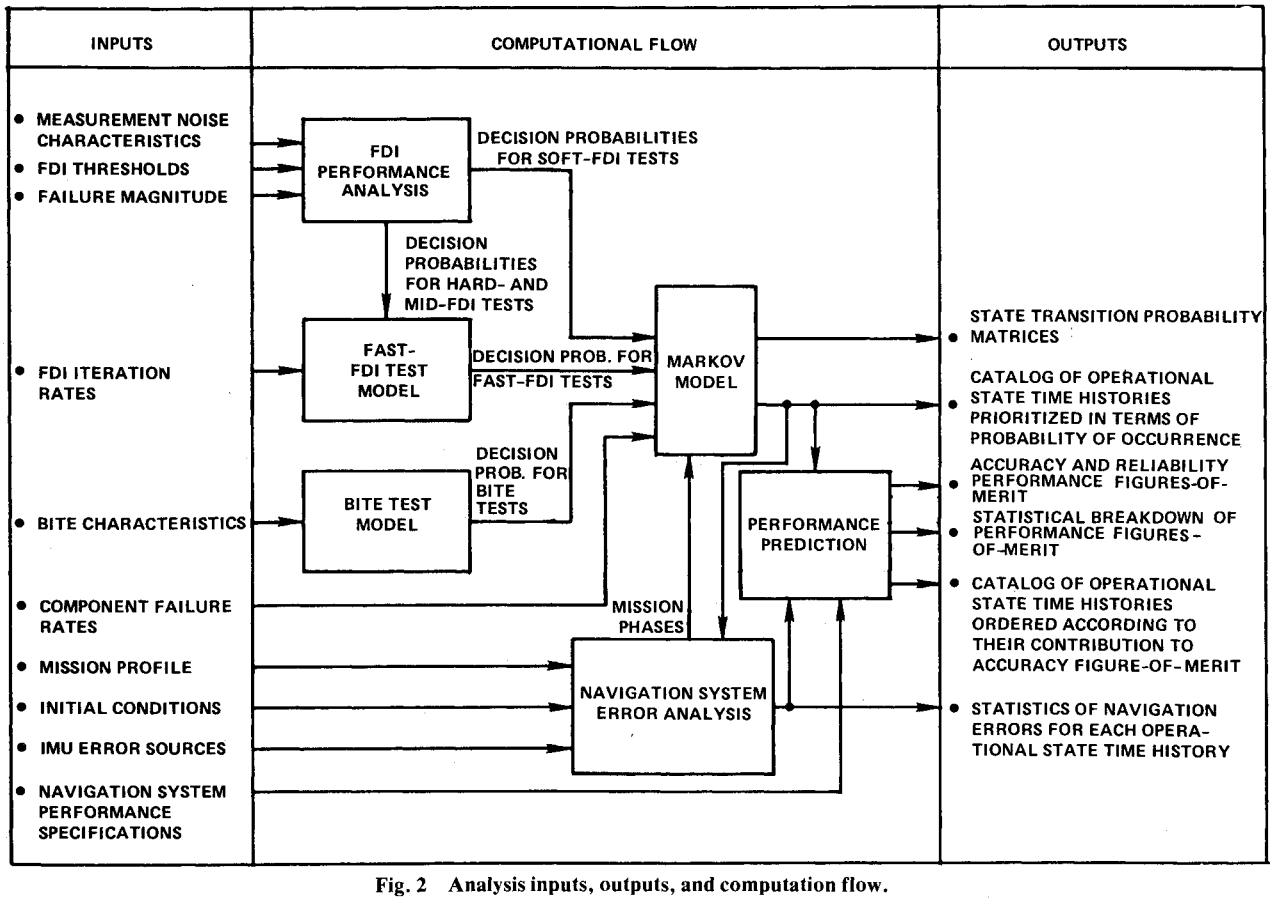

Fig. 2 Analysis inputs, outputs, and computation flow.

Table 5 Standard deviations of sensor measurement noise in dynamic (quiescent) environments

Test	Gyros, deg/h	Accelerometers, μg
Hard FDI	1200 (30)	350,000 (5000)
Mid FDI	25 (0.7)	7000 (85)
Soft FDI	0.25 (0.012)	64 (12)

Table 6 BITE characteristics

Type of BITE	Dynamic	Quiescent
Gyro BITE		
Coverage	0.25	0.25
False alarm probability, s^{-1}	7.7×10^{-9}	1.5×10^{-9}
Accelerometer BITE		
Coverage	0.25	0.25
False alarm probability, s^{-1}	3.9×10^{-9}	7.5×10^{-10}
Power supply BITE		
Coverage	0.90	0.90
False alarm probability, s^{-1}	1.9×10^{-8}	3.7×10^{-9}

Table 7 Component failure rates

Component	Failure rate, h^{-1}	
	Dynamic, $\times10^{-6}$	Quiescent, $\times10^{-6}$
Gyros	597	58
Accelerometers	162	16
Power supplies	922	183

Referring to the computational flow in Fig. 2, the navigation system error analysis is described in Ref. 4, and the FDI performance analysis is described in Ref. 8. The remaining computational blocks are described in Secs. II and III. Among the inputs indicated in Fig. 2, the FDI iteration rates are defined in Sec. I, and the mission profile, initial conditions, and the various sensor static and dynamic error sources are given in Ref. 4. The remaining inputs to the analysis are defined in the following paragraphs.

The noise which characterizes the inertial sensor measurements in the normal mode is a function of the dynamic environment as well as the filtering associated with each FDI test. Two mission environments are considered: one is characterized as dynamic and the other as quiescent. The five mission phases listed in Table 1 alternate between dynamic and quiescent environments. The noise which characterizes the sensor measurements in the dynamic (quiescent) environments is presented in Table 5.

The BITE characteristics are presented in Table 6. Coverage numbers indicate the percentage of failures which are correctly detected and identified by BITE tests. The false alarm rates are derived from a failure-modes-and-effects analysis of typical BITE circuitry.

The component failure rates are indicated in Table 7. These values are representative of currently available components for aerospace applications.

The navigation system accuracy specification was presented in Table 4. Since these values represent 3σ limits, this specification is equivalent to the requirement that the probability that one of the two largest errors exceeds these limits be less than 5.4×10^{-3}. This probability represents the requirement against which the accuracy figure of merit defined in Eq. (9) is to be measured. The system reliability specification is 0.9988. This corresponds to a requirement that the probability of vehicle loss be less than 1.2×10^{-3}. This probability represents the requirement against which the reliability figure of merit defined in Eq. (11) is to be measured.

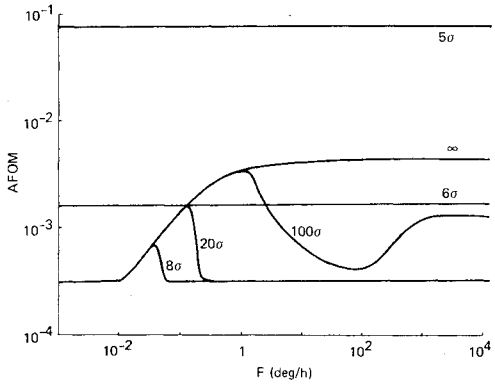

Fig. 3 Gyro AFOM in the presence of algorithmic FDI.

The inputs to the analysis defined in the previous paragraphs represent a baseline set of parameters (excluding, for the moment, the FDI thresholds and failure magnitude) for the redundant navigator and the geosynchronous orbit insertion mission. The numerical results presented in this paper focus on a small number of these parameters in order to illustrate particular uses of the analysis. All of the parameters influence system performance, however, and one of the major uses of the analysis is to quantify the sensitivity of this performance to each of these parameters.

The accuracy figure of merit (AFOM) for the redundant navigator without algorithmic FDI can be evaluated by considering the case of the redundant navigator with algorithmic FDI and infinitely large thresholds. This AFOM represents the envelope of the curves plotted as a function of gyro failure magnitude in Fig. 3 and is designated with an ∞. A similar curve can be obtained for a spectrum of accelerometer failure magnitudes. For failures below 0.01 deg/h, the AFOM reaches a lower bound that is insensitive to the gyro failure magnitude. Similar behavior is obtained for accelerometer failures less than 10 μg. These levels correspond to the bias stability values for the sensors. For failures larger than 100 deg/h, the AFOM in Fig. 3 is seen to reach an upper bound which is also insensitive to gyro failure magnitudes. Similar behavior is obtained for accelerometer failures which exceed $10^4\mu g$. These levels correspond to failure magnitudes which result in unit probability of mission loss.

The AFOM plotted in Fig. 3 was obtained by evaluating the sum indicated in Eq. (10) for a spectrum of failure magnitudes. The contribution to this sum which is associated with path 1, the normal operational state time history in which neither a failure nor a false alarm occurs during the mission, is 3.19×10^{-5}. The lower bound on the AFOM plotted in Fig. 3 is seen to be an order of magnitude larger than this. This is primarily due to the effects of power supply failures, which are covered only by BITE. The upper bound on the AFOM plotted in Fig. 3 reflects the additional effects of sensor failures which, in the absence of algorithmic FDI, are poorly covered by BITE.

Algorithmic FDI can be used to reduce the sensitivity of the redundant navigator's performance to failure magnitudes. If the FDI thresholds are chosen appropriately, this can be done without incurring a performance penalty in cases in which no failures or only small failures occur. Figure 3 also presents curves obtained for the case of the redundant navigator with algorithmic FDI. The parameters for these curves correspond to threshold levels, normalized to the standard deviation of the measurement noise (see Tables 5 and 6). For low thresholds (e.g., 5σ and 6σ), the AFOM are dominated by the presence of false alarms resulting in large AFOM's which are insensitive to failure magnitudes. False alarms contribute to the AFOM through two mechanisms: navigation system accuracy degrades (resulting in an increased AFOM) due to the removal of unfailed sensors, and because subsequent failures are less well covered. As the thresholds are increased

Table 8 Minimum detection levels

	Dynamic, deg/h			Quiescent, deg/h		
Threshold	Hard	Mid	Soft	Hard	Mid	Soft
5σ	9500	200	2.0	240	5.5	0.09
6σ	11,000	240	2.4	280	6.6	0.11
8σ	15,000	320	3.2	380	8.9	0.15
20σ	38,000	790	7.9	950	22	0.38
100σ	...	4000	40	4700	110	1.9

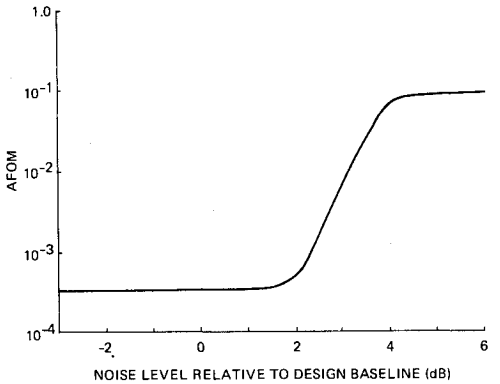

Fig. 4 Sensitivity of gyro AFOM to sensor measurement noise.

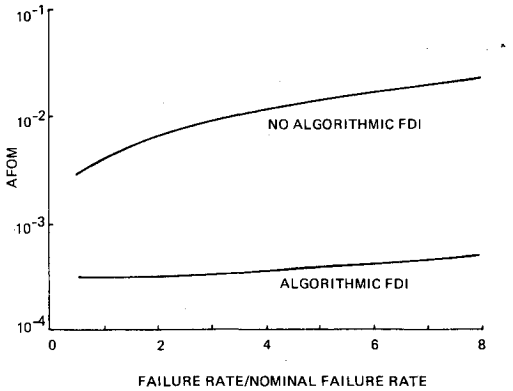

Fig. 5 Sensitivity of gyro AFOM to sensor failure rate.

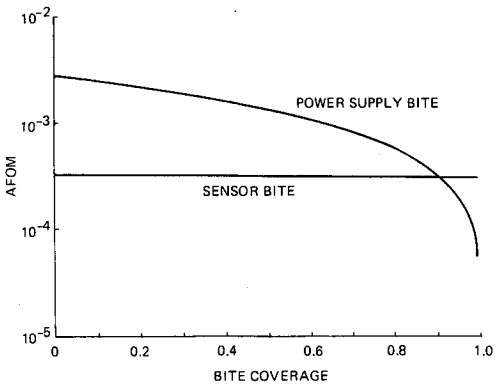

Fig. 6 Sensitivity of gyro AFOM to BITE coverage.

to approximately 7σ, the contribution of false alarms to the AFOM decreases monotonically until it constitutes less than 0.05% of the AFOM. As the thresholds are increased beyond this point, the minimum detectable failure levels also increase. These levels are shown in Table 8 for the various FDI tests in both dynamic and quiescent environments.

Examining the AFOM curves in Fig. 3, the AFOM's for 8σ and 20σ thresholds are seen to increase with failure magnitude until they reach a level at which they can be detected by the soft FDI test in quiescent environments, at which point the AFOM curves make a smooth transition back to a level which, for these threshold magnitudes, corresponds to the level observed for failure magnitudes less than 0.01 deg/h. As the threshold magnitudes are increased further, similar behavior is observed, but the level to which the AFOM returns begins to increase for large failure magnitudes. In the limit as the thresholds are increased, the no-algorithmic-FDI curve is approached.

Results similar to those presented in Fig. 3 are obtained when the AFOM is plotted against accelerometer failure magnitudes for various choices of thresholds, and when the RFOM is plotted against either gyro or accelerometer failure magnitudes. In general, however, the RFOM shows less sensitivity to failure magnitude than is indicated by the AFOM. Taken together, these results suggest that 8σ thresholds represent a reasonable choice. The slight sensitivity to failure magnitude which is indicated in Fig. 5 is exaggerated by the log scale of the abscissa. The range over which this sensitivity is indicated represents less than 0.001% of the range of failure magnitudes considered. For any reasonable distribution of $p(b)$, the assumption that the AFOM is insensitive to the sensor failure magnitude for these thresholds is justified.

Figure 4 indicates the sensitivity of the gyro AFOM to variations in the baseline sensor noise levels shown in Table 5. Noise levels from 3 dB below to 6 dB above the baseline are considered. As the noise level increases, the AFOM increases reflecting the consequences of false alarm contributions. The 8σ thresholds provide approximately 2 dB of noise margin before significant increases in the AFOM are experienced.

The sensitivity of gyro AFOM to gyro failure rate is shown in Fig. 5 over a range from one-half to eight times the nominal failure rate. The data presented is appropriate for relatively large failure magnitudes (10 deg/h or greater) and is shown for both a navigator with algorithmic FDI and for one without algorithmic FDI. It is evident from these data that the navigator without algorithmic FDI not only has a higher AFOM over this range of failure rates, but also that the AFOM is significantly more sensitive to the value of the failure rate than is the AFOM for the case with algorithmic FDI. The logarithmic abscissa of Fig. 5 obscures the linear relationship between AFOM and sensor failure rate. The data indicate that the sensitivity of the AFOM to uncertainty in the failure rate is reduced by two orders of magnitude when algorithmic FDI is used.

The sensitivity of the gyro AFOM to BITE coverage is indicated in Fig. 6. Because the algorithmic FDI provides effective coverage of sensor failures, the AFOM is insensitive to sensor BITE coverage. Failures of two of the three power supplies, on the other hand, are not covered by the algorithmic FDI. The AFOM thus indicates a significant sensitivity to power supply BITE coverage. Indeed, if coverage significantly higher than the baseline value of 0.90 is achieved, the lower bounds on the AFOM of Figs. 3 and 4 can be reduced to a level approaching the cost contribution of the normal mode.

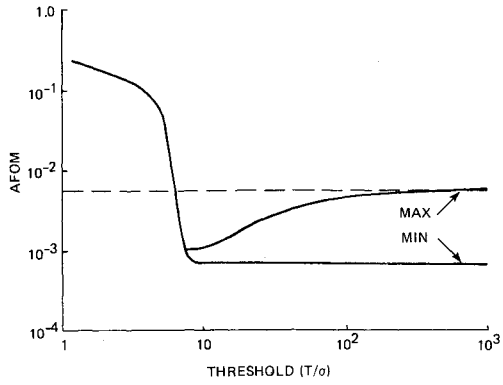

Fig. 7 Sensitivity of redundant navigator performance to thresholds.

Separate but structurally identical Markov models have been used to evaluate gyro and accelerometer figures of merit. This approach has the advantages of simplifying the analysis and reducing the number of states required in the Markov model in order to adequately model the system dynamics. Although much useful insight into system performance is obtained from these results, a single figure of merit for the redundant navigator (i.e., for the combined gyros and accelerometers) is desired. If it is assumed that gyro and accelerometer failures are independent events, the RIMU performance figures-of-merit may be approximated to a first order by

$$\text{AFOM} = \text{AFOM}_g p_a(1) + \text{AFOM}_a p_g(1) - c(1) p_a(1) p_g(1) \tag{14}$$

$$\text{RFOM} = \text{RFOM}_g p_a(1) + \text{RFOM}_a p_g(1) \tag{15}$$

where AFOM_g,AFOM_a are the gyro and accelerometer AFOM's, respectively; RFOM_g,RFOM_a are the gyro and accelerometer RFOM's, respectively; $p_a(1)$ is the probability of the (0,0,0,0,0) path for the accelerometers; $p_g(1)$ is the probability of the (0,0,0,0,0) path for the gyros; and $c(1)$ is the cost of the (0,0,0,0,0) path.

Using these approximations, the redundant navigator AFOM is plotted in Fig. 7 as a function of threshold magnitude for the redundant navigator. For larger thresholds, the AFOM is a function of failure magnitude and the upper and lower bounds of the AFOM are shown. These data suggest that thresholds of the order of 8-10σ are preferred. Although a very slight dependence upon failure magnitude is evident for these thresholds, almost any distribution of failure magnitudes will result in an overall AFOM equivalent to the minimum shown, since the maximum AFOM corresponds to a very narrow range of failure magnitudes (gyro failures in the range of 0.01 to 0.05 deg/h).

V. Conclusions

This paper has described a systematic approach to the problem of predicting the performance of a redundant strapdown inertial navigator. The approach combines the use of a Markov model of the redundant system with a linearized analysis of navigation system error statistics to evaluate scalar figures of merit for system accuracy and reliability. The sensitivity of system performance to uncertain system parameters can readily be determined. In addition to performance prediction, the analysis is particularly useful for determining the design margins which are inherent in the system, for evaluating design tradeoffs, for selecting free design parameters such as FDI thresholds, and for focusing attention on those aspects of the system design which afford the best opportunities for performance improvement.

The numerical results presented in this paper illustrate the various uses of the analysis. These results underline the close coupling which exists between system reliability and accuracy. The ability of FDI systems to desensitize system performance to failure effects, in much the same manner as feedback desensitizes control systems' performance to parameter variations, is clearly exhibited. The reduced sensitivity to poorly characterized system parameters such as distribution of sensor failure magnitudes, sensor failure rates, and sensor BITE coverage illustrated by this analysis permits overall redundant navigator performance to be predicted with high confidence, even though these underlying system characteristics cannot be experimentally verified.

The focus of this discussion has been on a specific redundant system and a specific application in order to describe the details of the implementation of the analysis and to present concrete numerical results. It should be clear from the discussion, however, that the approach is applicable to a wide spectrum of complex redundant systems.

References

[1] Gelb, A. (ed.), *Applied Optimal Estimation,* MIT Press, Cambridge, Mass., 1974, pp. 102-142.

[2] Bierman, G.J., *Factorization Methods for Discrete Sequential Estimation,* Academic Press, New York, 1977, pp. 191-201.

[3] Schweppe, F.C., *Uncertain Dynamic Systems,* Prentice-Hall, Englewood Cliffs, N.J., 1973, pp. 382-383.

[4] Harrison, J.V., Adams, M.B., Gai, E., Daly, K.C., and Ginter, S.D., "Performance of an Aided Redundant Navigator in Normal and Failure Modes," *Journal of Guidance and Control,* Vol. 3, No. 6, Nov.-Dec. 1980, pp. 481-486.

[5] Shooman, L., *Probabilistic Reliability: An Engineering Approach,* McGraw-Hill, New York, 1968, pp. 202-264.

[6] Baum, R.A., Morrison, G.E.S., and Peters, R.C., "A Redundant Inertial Navigation System for IUS," *Advances in Guidance and Control Systems Using Digital Techniques,* Paper No. 12, AGARD-CP-272, Aug. 1979.

[7] Daly, K.C., Gai., E., and Harrison, J.V., "Generalized Likelihood Test for FDI in Redundant Sensor Configurations," *Journal of Guidance and Control,* Vol. 2, No. 1, Jan.-Feb. 1979, pp. 9-17.

[8] Gai, E., Harrison, J.V., and Daly, K.C., "FDI Performance of Two Redundant Sensor Configurations," *IEEE Transactions on Aerospace and Electronic Systems,* Vol. AES-15, No. 3, May 1979, pp. 405-413.